Int J Thermophys (2011) 32:1887–1917
DOI 10.1007/s10765-011-1052-5

Measurements of Hydrogen Thermal Conductivity at High Pressure and High Temperature

S. Moroe · P. L. Woodfield · K. Kimura · M. Kohno · J. Fukai · M. Fujii · K. Shinzato · Y. Takata

Received: 9 February 2011 / Accepted: 12 July 2011 / Published online: 27 July 2011

Abstract The thermal conductivity for normal hydrogen gas was measured in the range of temperatures from 323 K to 773 K at pressures up to 99 MPa using the transient short hot-wire method. The single-wire platinum probes had wire lengths of 10 mm to 15 mm with a nominal diameter of 10 μm. The volume-averaged transient temperature rise of the wire was calculated using a two-dimensional numerical solution to the unsteady heat conduction equation. A non-linear least-squares fitting procedure was employed to obtain the values of the thermal conductivity required for agreement between the measured temperature rise and the calculation. The experimental uncertainty in the thermal-conductivity measurements was estimated to be 2.2 % ($k = 2$). An existing thermal-conductivity equation of state was modified to include the expanded range of conditions covered in the present study. The new correlation is

S. Moroe · K. Kimura · M. Kohno · Y. Takata
Department of Mechanical Engineering, Kyushu University, Nishi-ku, Fukuoka 819-0395, Japan
e-mail: shogo@gibbs.mech.kyushu-u.ac.jp

K. Kimura
e-mail: k_kimura_0114@yahoo.co.jp

M. Kohno
e-mail: kohno@mech.kyushu-u.ac.jp

Y. Takata
e-mail: takata@mech.kyushu-u.ac.jp

P. L. Woodfield (✉)
School of Engineering, Griffith University, Gold Coast Campus, QLD 4222, Australia
e-mail: p.woodfield@griffith.edu.au

P. L. Woodfield
International Research Center for Hydrogen Energy, Kyushu University, Nishi-ku,
Fukuoka 819-0395, Japan

applicable from 78 K to 773 K with pressures to 100 MPa and is in agreement with the majority of the present thermal-conductivity measurements within ±2 %.

Keywords High pressure · High temperature · Hydrogen · Thermal conductivity · Transient short hot-wire method

1 Introduction

The development of hydrogen fuel cell vehicles and the potential for hydrogen to play a key role as an energy carrier in the foreseeable future have intensified interest in the properties of hydrogen over a wide range of conditions. The study of hydrogen thermal conductivity has a history of over 140 years, probably beginning in the days of Maxwell when he correctly anticipated that it should be about seven times that of air [1]. The high thermal conductivity of hydrogen relative to other gases has been used as the characteristic for gas analysis in detectors for gas chromatography. It is also useful for measuring relative concentrations of *ortho*- and *para*-hydrogen [2,3] and for distinguishing among the different hydrogen isotopes [4]. Moreover, its high thermal conductivity makes hydrogen an effective heat carrier in cooling processes. In astrophysics, the thermal conductivity of hydrogen at extreme temperatures is required for study of the deep atmosphere of the larger planets and for heat transfer processes in the stars [5]. With the developing hydrogen economy, it is expected that the interest in hydrogen thermal conductivity will continue to increase over the next few years.

The volume of literature on the subject is large [6] but the range of well established primary data (verified by more than one study) is somewhat limited [7]. Moreover, high-temperature data in the high pressure region are virtually non-existent. The purpose of this study is to present some new measurements of hydrogen thermal conductivity at pressures to 99 MPa which, to the best knowledge of the authors, is 29 MPa higher than any other available measurements.

J. Fukai
Department of Chemical Engineering, Kyushu University, Nishi-ku, Fukuoka 819-0395, Japan
e-mail: jfukai@chem-eng.kyushu-u.ac.jp

M. Fujii · K. Shinzato · Y. Takata
Research Center for Hydrogen Industrial Use and Storage, National Institute of Advanced Industrial Science and Technology, 744 Mootoka, Nishi-ku, Fukuoka 819-0395, Japan
e-mail: fujii-motoo@aist.go.jp

K. Shinzato
e-mail: k.shinzato@aist.go.jp

Y. Takata
International Institute for Carbon-Neutral Energy Research (I2CNER),
Kyushu University, Fukuoka, Japan

2 Published Data Sets for Hydrogen Thermal Conductivity

A summary of the published data for hydrogen during the last 100 years has recently been given by Leachman et al. [6]. Further reviews of the older literature can be found in reports published by NIST in the 1970s and 1980s [8,9]. For low-density (dilute gas) hydrogen, Assael et al. [7] reviewed and correlated available reference-quality data. *Ab initio* theoretical data for hydrogen thermal conductivity can be found in a recent publication by Mehl et al. [10].

Figure 1 gives the positions on the pressure–temperature diagram where measurements of normal hydrogen thermal conductivity have been taken since 1966 (see Refs. [11–19]). The two largest data sets published for hydrogen thermal conductivity to date are those by Roder [11,12] (transient hot-wire method) and Roder and Diller [13] (guarded plate). Their data cover the entire liquid region and extend to a temperature of 316 K and pressures of 70 MPa. Unlike the majority of other authors, they considered both normal and para-hydrogen. In addition to the data shown in Fig. 1, Roder [11,12] also reported data for various concentrations of *para*- and *ortho*-hydrogen which are useful for calibration of thermal-conductivity meters used to measure the relative proportions of the two isomers [2,3]. Thermal-conductivity data for hydrogen with high reported accuracy have been taken using transient hot-wire instruments in the vicinity of room temperature [14–16]. The data by Hamrin and Thodos [17] and Hemminger [18] in Fig. 1 were measured with the coaxial cylinder method and the parallel-plate method, respectively. It is also worth mentioning here that high-temperature,

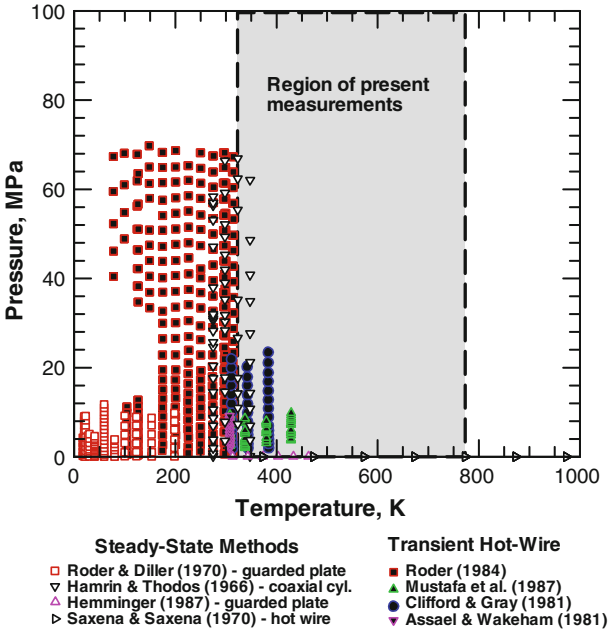

Fig. 1 Published data on hydrogen thermal conductivity [11–19] since 1966

high-pressure measurements of hydrogen thermal conductivity are currently in progress at NIST.

As is also clear from Leachman et al. [6], there appear to be no thermal-conductivity data published for pressures greater than 70 MPa. Since present commercial technology for compressed gas storage of hydrogen in vehicles has already reached 70 MPa, it is essential to have reliable thermal-conductivity data for higher pressures. For temperatures above 450 K, only the steady-state data of Saxena and Saxena [19] appear in Fig. 1. Earlier data for this region have been published [20], but it seems that nothing is available for high pressure.

3 Measurement Principle and Experimental Apparatus

The transient short hot-wire method [21–25] was used to measure the thermal conductivity in the present study. This technique is a variation of the usual transient hot-wire method [26] in that it employs only one short wire instead of two long wires of differing lengths. This makes the apparatus simpler, and it is ideal for high pressures and high temperatures since only a small pressure vessel is required. The challenge with the short hot-wire method is to compensate for the effect of heat conduction through the ends of the wire. This is taken into account through a high-precision numerical solution of the two-dimensional unsteady heat conduction equation [23]. The technique was originally proposed by Fujii et al. [21] and has been verified for use in liquids [21], electrically conducting fluids (coated wires) [22], and for gases [25,27].

Figure 2 gives a schematic diagram of the electrical circuit to simultaneously power and measure the resistance of the short hot wire. After the constant-current source (Keithley 2601) is switched on, the high-speed A/D convertor (National Instruments PXI-5922) simultaneously records the voltage drop across the standard resistor and the hot-wire probe. The voltage drop across the standard resistor provides a measurement of the electrical current, and through prior calibration of the hot wire, the voltage drop across the probe can be converted into the volume-averaged temperature of the wire. The measured transient temperature rise is influenced strongly by the thermal conductivity and thermal diffusivity of the sample fluid. Thus, these properties can be obtained via solution of the unsteady heat conduction equation. By completing the measurement within a short period of time (1 s in the present study), effects of natural convection are avoided. For the case of our hot-wire probe, the natural convection effect is estimated to become significant a few seconds after the heating [28]. This was confirmed experimentally for the case of helium at 97 MPa and 773 K.

Figure 3 shows an expanded diagram of the thermal-conductivity measurement apparatus. For the purposes of safe handling of high-pressure gas, the DC power supply, A/D board, pressure logger, and personal computer are located in a separate control room. The entire system is operated remotely. The AD board is operated at a sampling rate of 50 000 s^{-1} with a voltage measurement resolution of 24 bits. The pressure vessel for the thermal-conductivity cell has an inner diameter of 30 mm and a volume of 35 cm^3. Normal hydrogen gas (purity of 99.999 % as received) is compressed to a maximum pressure of 99 MPa and stored in an accumulator which is connected to the supply line for the thermal-conductivity apparatus. A series of valves

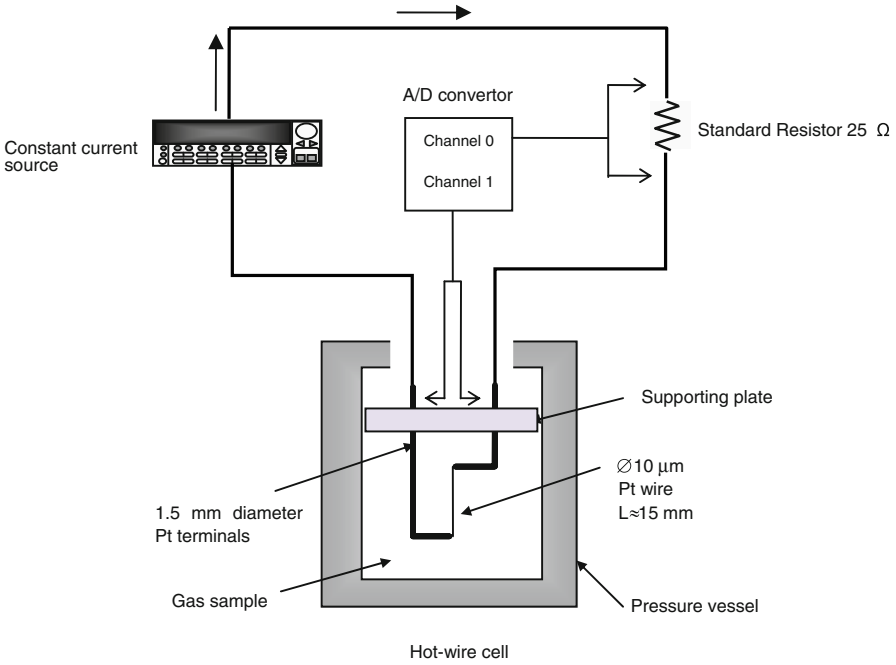

Fig. 2 Thermal-conductivity cell and measuring circuit

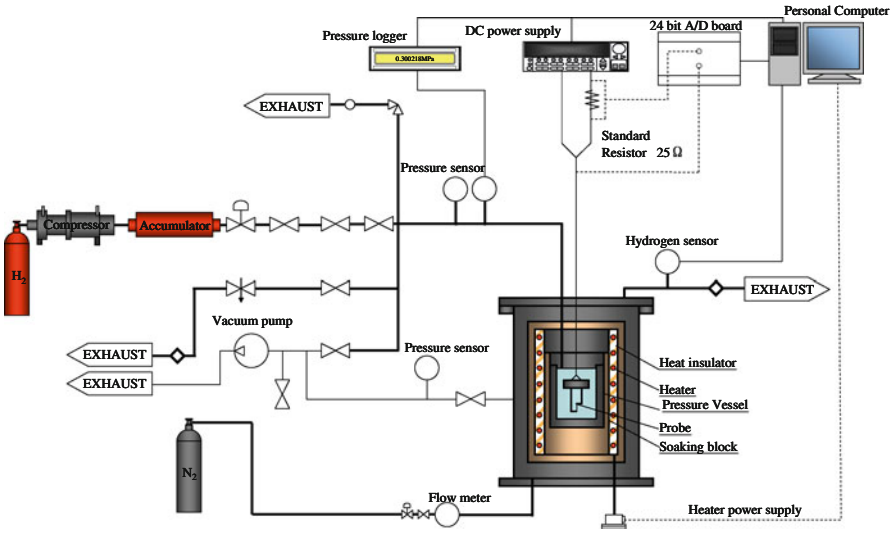

Fig. 3 Experimental setup

to restrict the maximum flow rate and a remotely operated pneumatic valve control the flow of hydrogen gas when filling the sample vessel. To lower the pressure, high-pressure gas can be released through the main exhaust line and the entire apparatus

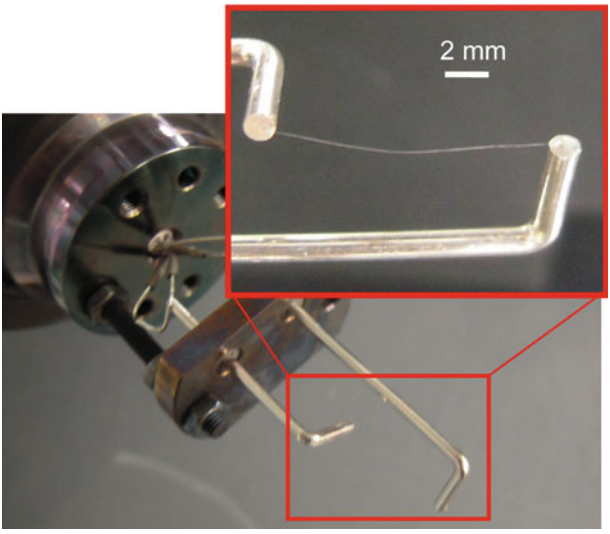

Fig. 4 Short hot-wire thermal-conductivity probe

can be finally evacuated using a vacuum pump to completely purge the system prior to inserting a fresh sample. The temperature of the sample vessel is controlled by a custom-built PID-controlled electric heating system. The sample pressure vessel is completely enclosed in a large copper block to promote a uniform temperature distribution. The copper block ('soaking block' in Fig. 3) is surrounded by the heating element, and the whole heating system is encased in an insulated container. Nitrogen gas is used for cooling, and the outlet gas is monitored to detect any hydrogen leaks from the pressure vessel. A standard platinum resistance thermometer (not shown in Fig. 3) calibrated according to the IST-90 temperature scale is inserted into the copper block. The pressure of the sample was measured with an oscillating quartz crystal absolute pressure transducer (Paroscientific Series 4000).

The heart of the apparatus is the short hot wire. A photograph of the probe is shown in Fig. 4. The material of the wire is platinum with a nominal diameter of 10 μm and is spot-welded to platinum terminals with a diameter of 1.5 mm. The power supply and measuring leads (also made of platinum) are spot-welded onto ends of the terminals following the principle of four-terminal resistance measurements. The use of the same material helps to reduce Seebeck effects and also reduces problems with differential thermal expansion at high temperatures. As mentioned above, the probe serves as both a heater and a resistance thermometer when the electrical current (DC) is supplied.

4 Physical Model and Analysis

Figure 5 shows the physical model for heat conduction in the hot-wire cell. The wire has a radius r_0 and length L and is positioned along the center line of a cylindrical vessel of radius R. The ends are attached to a terminal wire of radius r_1 and height h protruding from the bottom and top surfaces. Assuming axisymmetrical heat conduction and

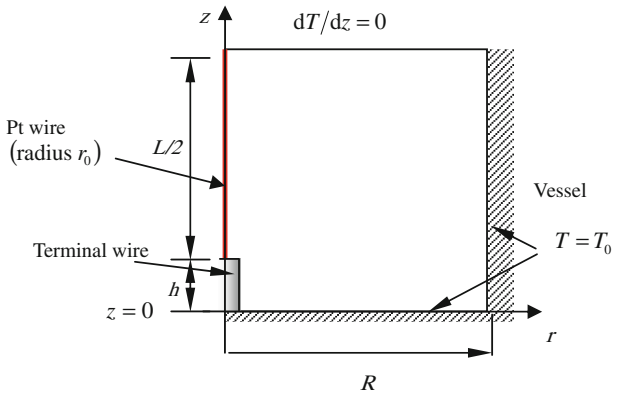

Fig. 5 Physical model for hot-wire cell

a plane of symmetry through the mid-height of the wire, the solution domain may be reduced from the whole region to that shown by Fig. 5. For this model, the governing equation is that for two-dimensional unsteady heat conduction and can be expressed in cylindrical coordinates as

$$\rho c \frac{\partial T}{\partial t} = \frac{1}{r}\frac{\partial}{\partial r}\left(r\lambda\frac{\partial T}{\partial r}\right) + \frac{\partial}{\partial z}\left(\lambda\frac{\partial T}{\partial z}\right) + q \tag{1}$$

$$q = Q/\pi r_0^2 \ (r \le r_0)$$
$$= 0 \ (r > r_0,\ z < h) \tag{2}$$

$$\frac{\partial T}{\partial z}|_{z=h+(L/2)} = 0 \tag{3}$$

$$T|_{r=R} = T|_{z=0} = T|_{t=0} = T_0 \tag{4}$$

For time $t > 0$, the electrical current is assumed to generate a constant and uniform volumetric heat source q in the short hot wire (In Eq. 2, Q is the heat generation rate per unit length of wire). Equation 3 represents the symmetry boundary condition at half the height of the wire ($z = h + (L/2)$). Equation 4 gives the initial condition and boundary conditions for the wall ($r = R$) and the bottom of the vessel ($z = 0$). The properties ρ, c, and λ are those of the wire for $r < r_0$ and those of the sample for $r > r_0$ where $z > h$. For $z < h$ the properties ρ, c, and λ are also those of platinum for $r < r_1$. It may be observed that there are some differences between the actual geometry shown in Fig. 4 and the geometry of the model. Nonetheless, the value of the radius R of the cylinder is taken to be the same as the actual value for the sample vessel. The length of the wire L and the radius of the wire r_0 are determined as effective values via calibration in a fluid with known properties as explained below. However, it turns out that with this technique, both L and r_0 come within a few percent of cathetometer and microscope measurements for the dimensions of the wire [21]. In the present calculation, radiation heat transfer is neglected. Equations 1 to 4 are solved by the finite volume method. Details of the solution method are described in Ref. [23].

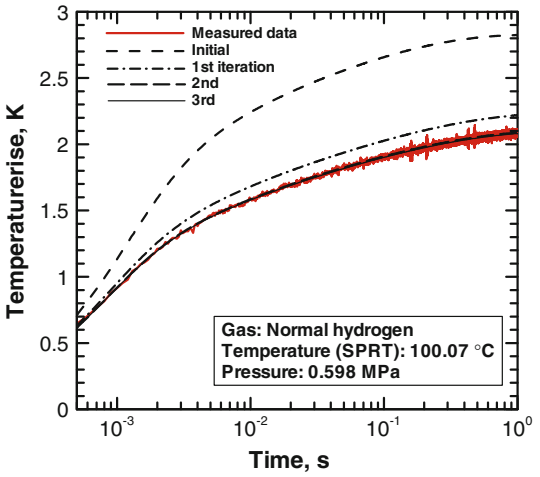

Fig. 6 Convergence of the present curve-fitting method

The errors of the numerical solutions have been estimated to yield an uncertainty of ±0.1 % of the determined thermal conductivity [23].

The thermal conductivity λ and thermal diffusivity α are evaluated through comparison of the numerical solution with the measured temperature rise. The method involves a number of calculations of the temperature rise in a non-linear least-squares curve fitting procedure so that finally the quantity S in the following equation is minimized.

$$S = \sum_{i=1}^{N_{\text{meas}}} \left(T_{\text{calc}(i)}\,(\lambda, \alpha) - T_{\text{meas}(i)} \right)^2 \tag{5}$$

In Eq. 5, N_{meas} is the total number of measured temperatures during transient heating, that is, approximately 50 000 for this work, where the heating time is 1 s. The curve-fitting procedure is described in detail in Ref. [23], so only a brief outline will be given here. Firstly, initial guesses are made for the values of λ and α and set as the parameters of the basic equations. Then the equation is solved to obtain the numerical values of the volumetric average temperature history $T_{\text{calc(i)}}(\lambda, \alpha)$. Pertubing the guessed value of λ by a small amount and then recalculating the temperature rise makes it possible to estimate the partial derivative of $T_{\text{calc(i)}}$ with respect to λ. In a similar manner, the partial derivative of $T_{\text{calc(i)}}$ with respect to α can be found. This forms the basis for a single iteration of the Gauss–Newton method for solving Eq. 5. Figure 6 gives an example of how the numerical curve approaches the experimental data as the curve-fitting algorithm progresses. The numerically obtained temperature rise shown by dark lines approaches the measured data each iteration, by updating the values of λ and α. In this case, the solution is converged by the third iteration and S takes a minimum value with a standard deviation of 0.013 K. The final values of λ and α are taken to be the sample thermal conductivity and thermal diffusivity, respectively.

5 Calibration of the Hot Wire

5.1 Temperature–Resistance Relationship

The temperature and subsequently the temperature rise of the wire are evaluated from the electrical resistance of the wire. It should be noted here that the electrical resistance of platinum wire varies not only with temperature but also with pressure in the high-pressure region [11]. The relationship between resistance, temperature, and pressure was expressed by the following algebraic equation:

$$R(T, P) = R(0, 0)\left(1 + \beta_1 T + \beta_2 T^2\right)(1 + \gamma P) \tag{6}$$

where $R(T, P)$ is the wire resistance at temperature T (°C) and pressure P (MPa), and $R(0, 0)$ is the resistance at 0 °C and 0 MPa. The temperature coefficients of resistance β_1 and β_2 and pressure coefficient γ were determined *in situ* by calibration against a standard platinum resistance thermometer (SPRT) inserted into the copper 'soaking block' surrounding the pressure vessel. The SPRT itself was calibrated using the IST-90 temperature scale. For the hot-wire probe, the calibration was performed while the sample vessel was filled with helium. The temperature of the pressurized sample vessel was adjusted in stages from 40 °C, to 500 °C, and the pressure was varied from 0.5 MPa to 100 MPa. After the apparatus temperature and pressure had become constant at the preset values, the temperature and pressure were measured accurately with the SPRT and pressure sensor, respectively. Simultaneously, the electrical resistance of the hot wire was measured. Figure 7 shows an example of the dependency of the electrical resistance on the pressure. As shown in the figure, a linear relation is observed. Furthermore, the gradient, that is, the pressure coefficient γ in Eq. 6 was found to be independent of the temperature. The value of γ is determined by the linear least-squares method to be -1.87×10^{-5} MPa^{-1}. The measurements in this work were performed using two different probes, probe A and probe B. From these data the coefficient $R(0, 0)$, β_1, and β_2 in Eq. 6 were determined and shown in Table 1.

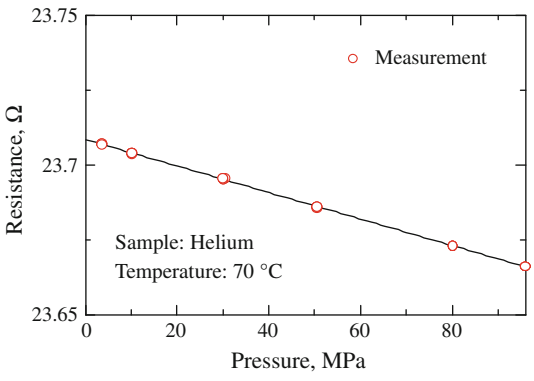

Fig. 7 Pressure dependence of the resistance of the platinum hot wire

Table 1 Calibration coefficients for hot wires

Probe	$R(0, 0)$ (Ω)	γ (MPa^{-1})	β_1 ($^\circ$C^{-1})	β_2 ($^\circ$C^{-2})
A	18.8973	-1.9×10^{-5}	3.634×10^{-3}	-3.489×10^{-7}
B	14.3974	-1.9×10^{-5}	3.899×10^{-3}	-5.993×10^{-7}

5.2 Effective Geometry for the Hot Wire

One of the recommended criteria (e.g., Ref. [7]) for the selection of primary reference data for developing equations of state for transport properties is that the measurements were taken with an absolute instrument. However, in recent years, some fluids such as toluene [29] and some of the noble gases at low density [30] have been so frequently and thoroughly investigated that relative instruments calibrated using such fluids can produce transport property data with an acceptable level of uncertainty. For example, May et al. [30] recently published data on hydrogen viscosity and other gases with a standard uncertainty of less than 0.1 % using an instrument calibrated relative to helium gas. They were able to justify their stated uncertainty based on the excellent agreement among the best available measurements and *ab initio* calculations of dilute-gas viscosity for helium [31].

As discussed in one of our previous studies [25], the transient short hot-wire method faces the challenge that uncertainties in the length measurement of the wire are significant because the wire is so short. For instance, ambiguities of the order of a few tenths of a millimeter associated with the precise location of the weld position are quite important for a 10 mm wire in contrast with a 100 mm wire where they may be acceptable. Moreover, as can be seen from a comparison of Figs. 4 and 5, there are some differences between the model geometry and the actual construction of the probe. Taking these factors into account, we have found that the best results for our instrument can be obtained if we measure the geometry of the short hot wires using a fluid of accurately known thermal conductivity and thermal diffusivity. For this purpose, we have selected helium gas.

In order to decide a suitable point of reference and to establish the level of uncertainty, we examined the published data for helium thermal conductivity. This is particularly important because the reputation of measured thermal-conductivity reference data has not always been good [26]. Figure 8 shows a comparison of published measurements in the vicinity of room temperature and reference correlations available from the literature. The correlation by Hands and Arp [32] is formulated into the NIST reference database [33]. Unlike the correlations by Bich et al. [34] and Kestin [35], the *ab initio* quantum mechanical calculations by Hurly and Moldover [31] have the feature that they did not involve the use of any measurements of the transport property data. Mustafa et al. [14], Assael et al. [36], and Kestin et al. [37] all used the transient hot-wire method. The parallel-plate data by Hemminger [18] show that the consistency among authors is not limited to a single method of measurement. Figure 8b shows the density dependence of the thermal conductivity of helium as measured in the region of temperatures shown in Fig. 8a. The solid line represents a

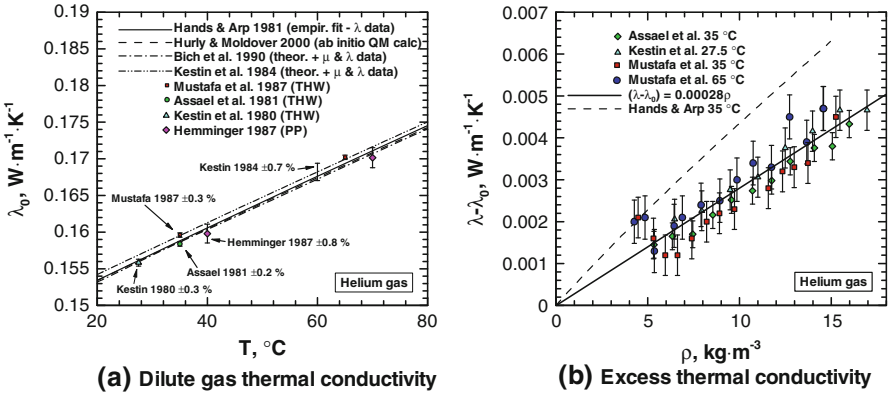

Fig. 8 Available reference data for helium thermal conductivity [14,18,31,32,34–37] (*THW* transient hot wire, *PP* parallel plate, *QM* quantum mechanical)

Table 2 Reference thermal-conductivity data used for determining L, d, and h

Probe	Fluid	T (K)	P (MPa)	λ ($\mathrm{W \cdot m^{-1} \cdot K^{-1}}$)
A	He	323.19	0.33 ± 0.015	0.1644 ± 0.0012
B	He	323.21	0.49 ± 0.015	0.1646 ± 0.0012

fit to the plotted data while the dotted line shows the trend of the correlation by Hands and Arp [32]. Based on this figure, the density dependence has only a small effect at low pressures. For example, at 35 °C a pressure of 1 MPa corresponds to a density of about 1.55 $\mathrm{kg \cdot m^{-3}}$ [38]. This causes an enhancement to the thermal conductivity of less than about 0.2 %. All of the data (both experimental and theoretical) in Fig. 8a are within ±0.6 % of the dilute-gas component of the correlation by Hands and Arp [32]. Based on the data shown in Fig. 8, we conservatively estimate that the uncertainty in the thermal conductivity of low-density helium in the range of temperatures from 20 °C to 80 °C is 0.7 % ($k = 2$). Moreover, although the correlation by Hands and Arp [32] has a larger stated uncertainty than the other correlations, it gives a good representation of the available reference data in this range. The values of the helium thermal conductivity used for calibration are listed in Table 2.

The other property required for calibration of the hot wire is the thermal diffusivity ($\alpha = \lambda/(\rho c_p)$). The uncertainty in the thermal diffusivity is related to the uncertainty in the thermal conductivity, density, and heat capacity. At low pressures, helium behaves like an ideal gas so that the uncertainty in the density and heat capacity become small. According to Arp and McCarty [39], the uncertainty in the density of helium is 0.1 % to a maximum of 0.25 % for the range of temperatures from 150 K to 400 K and pressures from 0 to 10 MPa. The heat capacity for the noble gases at low density has a simple theoretical relation involving the universal gas constant and the molar mass of the atom [40,41]. Therefore, the uncertainty in thermal diffusivity of low-pressure helium reference data is estimated to be 0.8 %. For the present study, however, the uncertainty in the thermal diffusivity is larger than this due to the uncertainty in our

Table 3 Calibration results of the effective dimensions of probe A

RUN	L (mm)	d (μm)	h (mm)
1	14.14	10.61	12.8
2	14.20	10.65	9.1
3	14.12	10.65	19.5
4	14.18	10.54	13.9
5	14.28	10.29	9.1
6	14.15	10.60	19.5
7	14.14	10.58	13.9
8	14.20	10.36	12.8
Ave.	14.18	10.53	13.8

pressure measurement (±15 kPa) (and hence the uncertainty in the density of helium in our apparatus) at the time of calibration. This increases the uncertainty in the thermal diffusivity for calibration of the present instrument to 5 %.

Having decided appropriate values for λ and α, we can now proceed to determine effective values for the apparatus constants, i.e., the wire diameter d, length L, and terminal length h using the non-linear least-squares fitting approach as described above (but with different unknown parameters). The volumetric average temperature rise $T_{\mathrm{calc}(i)}(L, d, h)$ is obtained for assumed parameters of L, d, and h, and it is compared with the temperature rise measured for the reference fluid at the corresponding time. The algorithm proceeds by updating the parameters until the following quantity S converges to a minimum value:

$$S = \sum_{i=1}^{N_{\mathrm{meas}}} \left(T_{\mathrm{calc}(i)}\,(L, d, h) - T_{\mathrm{meas}(i)}\right)^2 \rightarrow \min \tag{7}$$

In Eq. 7 N_{meas} is the number of temperatures measured during transient heating of the hot wire in the reference sample and $T_{\mathrm{meas}(i)}$ is the measured temperature rise of the hot wire corresponding to the measurement at time t_i. It is worth mentioning here that in our previous studies [23–25] the parameter h was zero. We have since found that for a low density gas, this additional variable gives a slightly better representation of the actual cell geometry. The calibration measurement was repeated eight times for probe A and four times for probe B. Tables 3 and 4 list the determined values for L, d, and h. Thermal-conductivity measurements indicated a low sensitivity to the selected value of h.

6 Measurement Procedure

After the temperature and pressure in the vessel reach a steady state at the desired values, a sequence of stepwise currents is supplied from the DC power supply to the short hot-wire probe. Figure 9 shows the typical pattern of electrical currents employed in

Table 4 Calibration results of the effective dimensions of probe B

RUN	L (mm)	d (μm)	h (mm)
1	11.35	9.80	2.83
2	11.32	9.96	2.98
3	11.32	9.89	2.97
4	11.29	10.05	2.92
Ave.	11.32	9.92	2.93

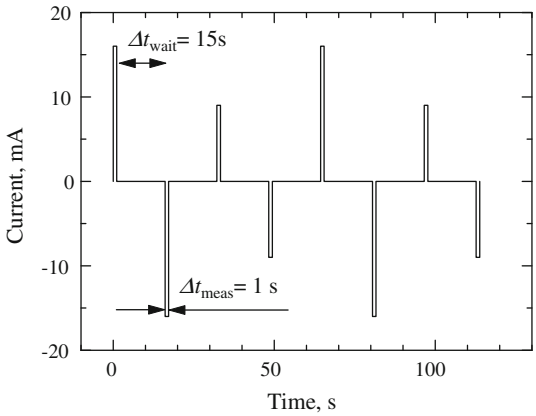

Fig. 9 Sequence of electrical currents applied to hot-wire probe

the present study. A negative current indicates that the polarity of the current has been reversed. Basically two different magnitudes of current are used. For the example in Fig. 9 the magnitudes are 17 mA and 9 mA. The larger of the two is the measuring current for the temperature rise of the probe from which the thermal conductivity is determined. The smaller current serves the purpose of providing a means to extrapolate to find the initial resistance of the unheated wire. Reversing the polarity is done automatically in the computer program which sends a command to the current source to output a negative current. As explained in Ref. [25], this technique is very effective in eliminating the effect of small offset voltages arising through zero errors in the A/D board and/or Seebeck effects at connections of dissimilar materials in the measuring circuit.

As can be seen in Fig. 9, there are four large pulses and four small pulses, each with a duration of $\Delta t_{\text{meas}} = 1$ s. Figure 10 shows an example of resistances measured using two large pulses and two small pulses. The different shade lines indicate forward and reverse polarities. It is worth noting here that the level of noise is larger than our previous (low-pressure) study [25] due to the long cables (20 m) required for remote operation of the high-pressure apparatus. Moreover, to reduce the size of the figure, only about 20 % of the measured points are plotted in Fig. 10. It is apparent that the resistances measured with forward and reverse polarities are slightly offset from each other ($\sim$0.005 Ω). This is the result of a small bias voltage in the circuit and confirms the value of reversing the polarity to obtain an accurate measurement. Figure 10 also shows the effect of extrapolating the measured resistance to zero power against I^2R for each point in time. The average of this extrapolation is taken to correspond to the

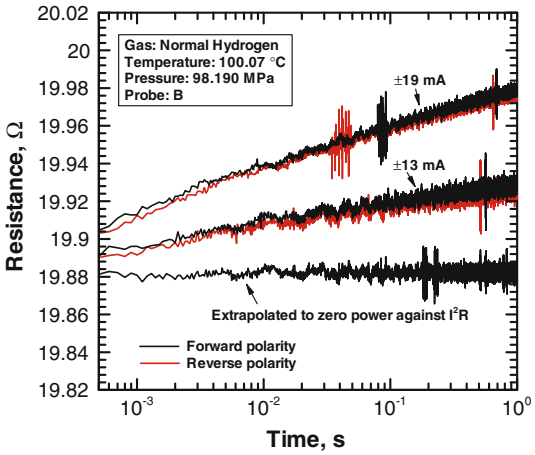

Fig. 10 Measured transient resistances for the hot wire before ensemble averaging

initial temperature of the unheated wire. The theoretical basis for obtaining the initial resistance in this manner is discussed in detail in Ref. [25]. For the present A/D converter, this technique was found to be more reliable than simply using a small current with the assumption that the wire was not heated.

To finally provide a measured temperature rise for determining the thermal conductivity, an ensemble average of the resistances measured with the four larger pulses was used. This reduces the level of noise in the data and, as mentioned above, it compensates for any bias voltages resulting from thermal differences in the circuit. Because the sampling rate of the A/D convertor was 50 000 s^{-1}, determining the time origin for the temperature rise for each heating pulse was not a serious issue. Also, the synchronization of the two channels for simultaneous measurement of the voltage and current was confirmed to be at least as good as ± 0.02 ms.

Equation 6 is used to convert the ensemble-averaged resistance to a temperature rise. Figure 11 shows two examples of data for measurement of the hydrogen gas thermal conductivity. These two figures represent the extremes of conditions considered. At low pressures (Fig. 11a) the temperature rise is far from a straight line in contrast with the high-pressure measurement (Fig. 11b). The reasons for this difference are that the thermal diffusivity is much smaller for the higher-pressure case and the heated region of the fluid does not reach the wall of the vessel. The data shown in Fig. 11b correspond to the resistance measurements shown in Fig. 10. Comparing Figs. 10 and 11, the reduction in noise due to ensemble averaging is apparent in Fig. 11. The dark line (calculation) is the result of applying the curve-fitting procedure (outlined above) in order to find the thermal conductivity of the gas.

7 Uncertainty Analysis

The uncertainty analysis used for the present transient short hot-wire method is explained in detail in Ref. [25]. The general procedure follows the ISO guideline [42]. In order to do this, the thermal conductivity is expressed as

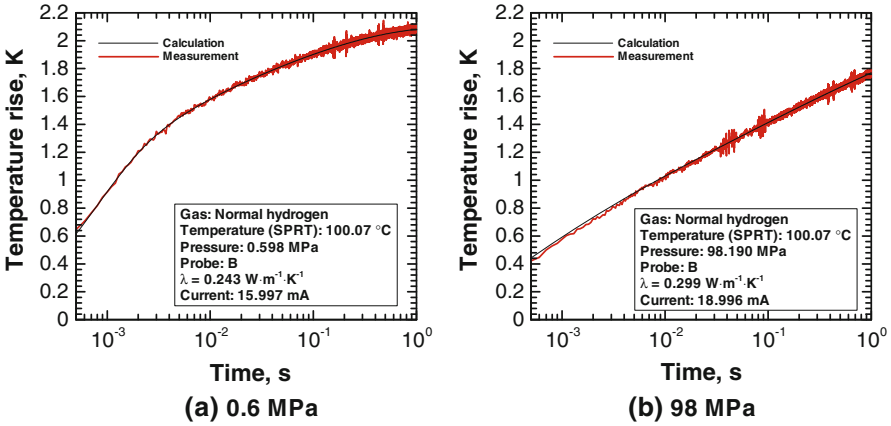

Fig. 11 Example transient temperature rises for hydrogen at different pressures

$$\lambda = f\left(X_1, X_2, \ldots, X_N\right) \tag{8}$$

where X_1, X_2, …, X_N are input parameters (experimental inputs) for the physical model and $f()$ is the solution to Eq. 5. The combined standard uncertainty $u_c(\lambda)$ is given by

$$u_{\mathrm{c}}^2\left(y\right) = \sum_{i=1}^{N} \left(\frac{\partial f}{\partial x_i}\right)^2 u^2\left(x_i\right) \tag{9}$$

where $u^2(x_i)$ is the estimated variance of x_i (the input estimate for X_i) and cross-correlation terms have been neglected (or eliminated [25]). Since $f()$ in Eq. 8 is a numerical solution, the partial derivatives for Eq. 9 are determined using

$$\frac{\partial f}{\partial x_i} u\left(x_i\right) \approx \frac{1}{2}\left\{f\left[x_1, \ldots, x_i + u\left(x_i\right), \ldots, x_N\right] - f\left[x_1, \ldots, x_i - u\left(x_i\right), \ldots, x_N\right]\right\} \tag{10}$$

Table 5 gives the estimated standard uncertainties. The uncertainties in the length and diameter of the wire are due to a combination of the uncertainty in the properties of helium listed in Table 2 and the uncertainties in the calibration procedure. Combining the values in Table 5 according to Eq. 9 and then expressing the result for $k = 2$ gives an overall uncertainty in the thermal conductivity of 2.2 %.

8 Thermal-Conductivity Measurement Results

Two kinds of gases were investigated over a wide range of temperatures and pressures, that is, helium and hydrogen. The former was used as a reference or standard gas with accurately known thermophysical properties. As shown in Fig. 8, the validity

Table 5 Combined standard uncertainty in λ

	Est. uncertainty	Effect on λ $u_{\lambda i}$ (%)
Temperature rise	0.0038 K	0.008
Initial wire temperature	0.010 K	0.5
Starting time	0.05 ms	0.01
Power to wire	0.05 %	0.05
Wire diameter	3.0 %	0.45
Wire length	1.0 %	0.79
Cell diameter	0.3 mm	0.003
Platinum thermal conductivity	1.50 %	0.01
Platinum heat capacity (ρc_p)	2.50 %	0.008
Combined		1.1
k= 2		2.2

of helium thermal-conductivity reference data could be confirmed among authors for low pressures in the vicinity of room temperature. At higher pressures the uncertainty in the helium reference correlations may increase to 4 % or 5 % [32,33]. The thermal conductivity of hydrogen gas is the main target for measurement over a wide range of temperature and pressure. Only thermal-conductivity measurements will be reported here since the reliability of the present thermal-diffusivity measurements could not be established. This is a common challenge for transient hot-wire methods [43]. It is worth mentioning that uncertainties in the thermal diffusivity of the reference gas for calibration were found to have little influence on the measured thermal conductivity.

8.1 Thermal Conductivity of Helium

The thermal conductivity of helium gas was measured in the range of temperature from 50 °C to 300 °C and pressures to 99 MPa. Table 6 lists the measurements. Figure 12 shows the deviations of the present thermal-conductivity measurements from the wide-ranging correlation by Hands and Arp [32]. All measured data agree well with the thermal-conductivity surface by Hands and Arp within a deviation of ±1.5 % except for the high-pressure region beyond 70 MPa where deviations of around 2 % are observed as shown in Fig. 12. This is well within the estimated uncertainty of 4 % proposed by Hands and Arp for their correlation.

8.2 Thermal Conductivity of Hydrogen

The thermal conductivity of hydrogen was measured for temperatures from 50 °C to 500 °C and pressures up to 99 MPa. Tables 7 and 8 list the measurements and the corresponding conditions. Table 7 contains measurements taken with probe A and Table 8 for probe B. Five isotherms are given for probe B, and one isotherm is

Table 6 Measured helium thermal conductivity (Probe B)

P (MPa)	T (K)	λ ($W \cdot m^{-1} \cdot K^{-1}$)
323.2 K isotherm		
5.030	323.20	0.1674
5.030	323.20	0.1675
5.030	323.20	0.1677
5.030	323.19	0.1676
10.055	323.19	0.1696
10.055	323.19	0.1695
10.055	323.19	0.1695
10.055	323.19	0.1694
29.887	323.19	0.1783
29.886	323.19	0.1782
29.885	323.19	0.1784
29.885	323.19	0.1786
50.067	323.21	0.1870
50.070	323.21	0.1872
50.072	323.21	0.1872
50.075	323.21	0.1870
70.102	323.21	0.1960
70.105	323.21	0.1960
70.109	323.21	0.1961
70.112	323.21	0.1964
98.251	323.21	0.2089
98.254	323.21	0.2085
98.259	323.21	0.2085
98.263	323.21	0.2086
373.2 K isotherm		
5.137	373.23	0.1850
5.137	373.22	0.1853
5.137	373.23	0.1845
10.114	373.23	0.1866
10.114	373.23	0.1868
10.114	373.23	0.1866
30.214	373.22	0.1948
30.214	373.22	0.1945
30.213	373.22	0.1948
49.994	373.22	0.2033
49.992	373.22	0.2028
49.990	373.22	0.2028
69.937	373.23	0.2140

Table 6 continued

P (MPa)	T (K)	λ ($W \cdot m^{-1} \cdot K^{-1}$)
69.936	373.23	0.2139
69.936	373.23	0.2138
97.514	373.23	0.2284
97.516	373.23	0.2277
97.527	373.23	0.2275
473.3 K isotherm		
5.261	473.28	0.2173
5.261	473.27	0.2169
5.260	473.27	0.2166
10.173	473.27	0.2193
10.172	473.27	0.2187
10.172	473.27	0.2183
30.084	473.28	0.2252
30.085	473.28	0.2251
30.085	473.28	0.2260
50.076	473.27	0.2321
50.078	473.27	0.2322
50.080	473.27	0.2317
70.131	473.27	0.2428
70.135	473.27	0.2422
70.138	473.27	0.2419
99.160	473.29	0.2472
99.148	473.27	0.2558
99.151	473.27	0.2549
99.156	473.27	0.2552
573.3 K isotherm		
5.197	573.25	0.2478
5.199	573.25	0.2472
5.200	573.25	0.2477
10.292	573.25	0.2503
10.294	573.25	0.2496
10.295	573.25	0.2496
30.146	573.25	0.2552
30.146	573.24	0.2549
30.149	573.25	0.2558
50.095	573.25	0.2609
50.100	573.25	0.2599
50.100	573.24	0.2618
70.129	573.24	0.2675
70.160	573.25	0.2680
70.165	573.25	0.2662

Table 6 continued

P (MPa)	T (K)	λ ($W \cdot m^{-1} \cdot K^{-1}$)
97.066	573.24	0.2798
97.071	573.24	0.2805
97.072	573.24	0.2792
672.9 K isotherm		
5.413	672.90	0.2765
5.416	672.90	0.2770
5.417	672.89	0.2774
10.409	672.89	0.2788
10.412	672.89	0.2790
10.414	672.89	0.2784
30.054	672.89	0.2843
30.064	672.88	0.2852
30.085	672.88	0.2823
50.178	672.89	0.2895
50.182	672.89	0.2888
50.184	672.88	0.2882
70.068	672.88	0.2930
70.074	672.88	0.2949
70.081	672.88	0.2948
98.224	672.87	0.3057
98.231	672.87	0.3054
98.230	672.87	0.3055
771.9 K isotherm		
1.059	771.94	0.2998
1.068	771.94	0.3028
1.071	771.94	0.3022
1.074	771.94	0.3040
3.001	771.94	0.3012
3.003	771.94	0.3055
3.005	771.93	0.3046
3.008	771.93	0.3049
5.202	771.93	0.3079
5.204	771.92	0.3065
10.197	771.91	0.3094
10.199	771.91	0.3093
30.345	771.90	0.3126
30.348	771.90	0.3102
30.350	771.90	0.3130
50.118	771.89	0.3162
50.125	771.89	0.3184

Table 6 continued

P (MPa)	T (K)	λ ($W \cdot m^{-1} \cdot K^{-1}$)
50.128	771.89	0.3182
70.299	771.89	0.3237
70.303	771.89	0.3173
70.305	771.89	0.3224
99.452	771.89	0.3302
99.460	771.89	0.3299
99.462	771.89	0.3321

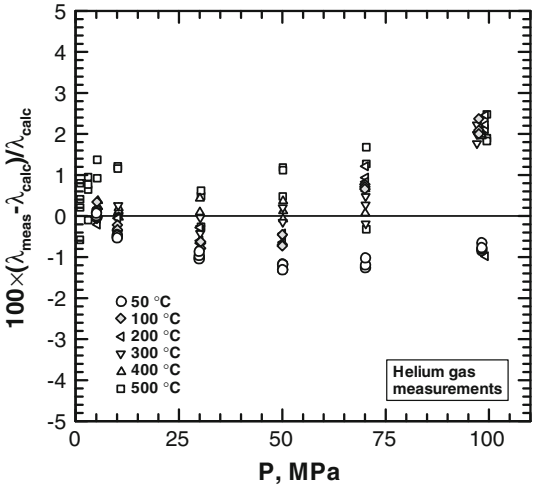

Fig. 12 Deviation of present thermal-conductivity measurements for helium gas from the correlation by Hands and Arp [32]

given for probe A. For any particular condition of temperature and pressure, thermal-conductivity measurements were repeated three to five times consecutively (over a period of 30 min to an hour) as listed in the tables. In the tables, the thermal conductivity is given to the fourth decimal place not to indicate accuracy but rather to enable a comparison of the variation among repeated measurements. The uncertainty in the thermal-conductivity measurements is estimated to be 2.2 % as discussed above. For the measurements collected using probe B, the 373.2 K isotherm was measured first of all and then re-measured towards the end of data collection to confirm consistency.

9 Unexpected Measurement Issues

It is worth mentioning here that an attempt was also made to take high-temperature measurements with probe A. The results are not included because after a considerable time at high temperature, the resistance/temperature calibration of probe A started to change and finally the wire failed completely. Moreover, upon opening the vessel, it was found that small metallic crystals had formed on the wire. The origin of the crystals was traced to a high-temperature ceramic bond which was used to help

Table 7 Measured hydrogen thermal conductivity (Probe A)

P (MPa)	T (K)	λ ($W \cdot m^{-1} \cdot K^{-1}$)
0.261	323.20	0.1971
0.261	323.20	0.1970
0.266	323.20	0.1971
0.267	323.20	0.1973
0.266	323.20	0.1971
5.188	323.20	0.2031
5.190	323.20	0.2031
5.193	323.19	0.2032
5.191	323.19	0.2032
5.186	323.20	0.2029
10.100	323.19	0.2065
10.095	323.20	0.2065
10.094	323.19	0.2067
10.087	323.20	0.2067
10.084	323.20	0.2067
19.987	323.20	0.2147
19.998	323.20	0.2146
20.000	323.20	0.2142
19.989	323.20	0.2142
19.980	323.21	0.2147
40.020	323.20	0.2313
40.011	323.20	0.2304
39.993	323.20	0.2306
39.984	323.20	0.2311
40.006	323.20	0.2312
59.985	323.20	0.2488
59.986	323.20	0.2482
59.968	323.20	0.2483
59.948	323.20	0.2488
59.935	323.21	0.2488
80.034	323.20	0.2657
80.012	323.20	0.2648
79.984	323.20	0.2654
79.963	323.20	0.2659
80.001	323.20	0.2659
97.745	323.20	0.2813
97.707	323.20	0.2804
97.716	323.20	0.2820
97.753	323.20	0.2816
97.762	323.20	0.2814

Table 8 Measured hydrogen thermal conductivity (Probe B)

P (MPa)	T (K)	λ ($W \cdot m^{-1} \cdot K^{-1}$)
373.2 K isotherm		
0.599	373.23	0.2224
0.599	373.22	0.2225
0.598	373.22	0.2223
0.598	373.22	0.2224
5.171	373.23	0.2262
5.170	373.22	0.2262
5.170	373.22	0.2260
5.170	373.22	0.2261
10.219	373.23	0.2296
10.219	373.23	0.2295
10.219	373.23	0.2296
10.219	373.23	0.2298
30.119	373.23	0.2438
30.120	373.23	0.2437
30.120	373.23	0.2433
30.122	373.23	0.2432
50.144	373.23	0.2589
50.144	373.23	0.2588
50.144	373.23	0.2589
70.084	373.22	0.2757
70.084	373.22	0.2758
70.086	373.22	0.2758
98.197	373.22	0.2988
98.193	373.23	0.2983
98.190	373.23	0.2987
98.187	373.22	0.2983
423.3 K isotherm		
0.400	423.27	0.2421
0.402	423.27	0.2431
0.403	423.26	0.2426
0.404	423.26	0.2418
5.113	423.26	0.2477
5.114	423.26	0.2476
5.114	423.25	0.2475
10.104	423.26	0.2499
10.105	423.25	0.2494
10.105	423.25	0.2502
30.087	423.25	0.2620
30.087	423.25	0.2619

Table 8 continued

P (MPa)	T (K)	λ ($W \cdot m^{-1} \cdot K^{-1}$)
30.087	423.25	0.2615
50.100	423.26	0.2771
50.100	423.26	0.2762
50.102	423.25	0.2764
70.147	423.25	0.2939
70.150	423.25	0.2927
70.155	423.25	0.2923
96.975	423.25	0.3140
96.978	423.25	0.3137
96.980	423.25	0.3142
573.3 K isotherm		
0.365	573.28	0.2934
0.367	573.28	0.2929
0.369	573.28	0.2931
5.202	573.27	0.3043
5.202	573.27	0.3057
5.202	573.27	0.3047
10.155	573.27	0.3066
10.155	573.27	0.3072
10.156	573.27	0.3066
30.167	573.27	0.3171
30.167	573.27	0.3173
30.167	573.27	0.3175
50.208	573.26	0.3253
50.204	573.27	0.3274
50.202	573.26	0.3283
70.114	573.27	0.3387
70.106	573.27	0.3381
70.099	573.27	0.3376
97.001	573.26	0.3548
96.990	573.26	0.3549
96.979	573.26	0.3560
473.3 K isotherm		
0.407	473.28	0.2609
0.408	473.29	0.2613
0.408	473.28	0.2610
0.409	473.28	0.2611
5.166	473.28	0.2673
5.167	473.28	0.2670
5.167	473.28	0.2671

Table 8 continued

P (MPa)	T (K)	λ ($W \cdot m^{-1} \cdot K^{-1}$)
10.065	473.27	0.2681
10.065	473.27	0.2687
10.065	473.28	0.2691
30.123	473.27	0.2799
30.124	473.27	0.2800
30.124	473.27	0.2803
50.176	473.28	0.2940
50.178	473.28	0.2937
50.179	473.28	0.2920
70.155	473.27	0.3079
70.156	473.27	0.3088
70.160	473.27	0.3069
97.460	473.27	0.3282
97.459	473.27	0.3262
97.457	473.27	0.3277
672.9 K isotherm		
0.304	672.89	0.3296
0.304	672.89	0.3290
0.305	672.89	0.3290
0.306	672.89	0.3287
5.147	672.88	0.3430
5.143	672.88	0.3429
5.140	672.88	0.3440
5.137	672.88	0.3420
10.061	672.88	0.3445
10.060	672.88	0.3456
10.059	672.88	0.3459
30.074	672.87	0.3514
30.063	672.87	0.3522
30.056	672.87	0.3514
50.118	672.87	0.3625
50.107	672.88	0.3616
50.096	672.87	0.3600
70.044	672.88	0.3699
70.030	672.88	0.3711
70.012	672.88	0.3693
98.109	672.87	0.3873
98.074	672.87	0.3853
98.041	672.87	0.3854

Table 8 continued

P (MPa)	T (K)	λ ($W \cdot m^{-1} \cdot K^{-1}$)
373.2 K (Repeat)		
4.315	373.23	0.2265
4.316	373.23	0.2258
4.316	373.23	0.2256
10.127	373.23	0.2291
10.126	373.24	0.2296
10.126	373.23	0.2289
30.053	373.23	0.2422
30.052	373.23	0.2428
30.052	373.23	0.2427
49.936	373.23	0.2599
49.936	373.23	0.2582
49.936	373.23	0.2587
69.998	373.23	0.2753
69.997	373.23	0.2756
69.998	373.23	0.2751
97.555	373.23	0.3001
97.558	373.23	0.2995
97.560	373.23	0.2989
771.9 K isotherm		
0.378	771.92	0.3679
0.381	771.92	0.3675
0.383	771.92	0.3671
0.386	771.92	0.3678
5.144	771.91	0.3835
5.140	771.92	0.3835
5.136	771.92	0.3832
10.109	771.91	0.3825
10.100	771.91	0.3836
10.092	771.91	0.3825
10.086	771.91	0.3838
30.058	771.91	0.3900
30.036	771.90	0.3906
30.014	771.91	0.3888
29.994	771.90	0.3905
49.932	771.90	0.3973
49.904	771.90	0.3973
49.879	771.91	0.3964
70.520	771.91	0.4053
70.484	771.90	0.4065

Table 8 continued

P (MPa)	T (K)	λ ($W \cdot m^{-1} \cdot K^{-1}$)
70.444	771.90	0.4037
70.405	771.90	0.4080
99.205	771.90	0.4188
99.143	771.90	0.4168
99.008	771.90	0.4170
98.954	771.90	0.4176

support the platinum terminal wires. The crystals were analyzed and found to be pure aluminum. The failure of probe A wire was attributed to having too much tension from the time of welding. Therefore, probe B was constructed as shown in Fig. 4 without significant tension. The low-temperature measurements using Probe A listed in Table 7 are believed to be unaffected by these issues since they were taken before the probe started to show signs of unexpected behavior. The consistency of the repeated 373.2 K isotherm for probe B listed in Table 8 indicates that (unlike probe A) the reliability of probe B for thermal-conductivity measurement did not diminish over time.

10 Correlation of Hydrogen Thermal-Conductivity Data

The present data extend beyond the existing range of measured thermal conductivities for hydrogen gas. Therefore, it is valuable to represent the new data in the form of an expanded correlation. A commonly used approach for a wide-range correlation of thermal-conductivity data is to divide the thermal conductivity into a dilute gas term (i.e., the zero-density limit) λ_0 which is only a function of temperature, a term that shows the effect of fluid density $\Delta\lambda_{\text{excess}}$, and a critical enhancement term $\Delta\lambda_{\text{crit}}$.

$$\lambda(\rho, T, x) = \lambda_0(T, x) + \Delta\lambda_{\text{excess}}(\rho, T) + \Delta\lambda_{\text{crit}}(\rho, T) \tag{11}$$

This approach was followed by Roder [11] for correlating hydrogen thermal-conductivity data in the range of temperature from 78 K to 423 K with pressures to 70 MPa. Extrapolating Roder's correlation to the region covered by the present measurements showed promising results with a maximum deviation of only about 4 %. Therefore, we have attempted to modify the basic correlation proposed by Roder [11]. For the effect of the mole fraction of para-hydrogen, x, Roder recommended a linear mixing rule,

$$\lambda_0(T, x) = \lambda_{\text{norm}}(T) + [(x - 0.25)/0.75] \times \Delta\lambda_{\text{p-n}} \tag{12}$$

where $\Delta\lambda_{\text{p-n}}$ is the difference between the thermal conductivity of para-hydrogen and normal hydrogen. For dilute-gas normal hydrogen, Roder used the table of theoretical calculations by Hanley et al. [44] with a small correction factor to account for the deviations between his measurements and the theoretical data. For the present

Table 9 Coefficients for present correlation

i	C_i	D_i	E_i
1	0.0842	1.275	0.79
2	0.0198	−2.74	2.6
3	0.0118	3.46	0.31

correlation, we fitted the following equation (assuming $F(T) = 1$) to the data in the table for normal dilute hydrogen by Hanley et al. [44].

$$\frac{\lambda_{\text{norm}}(T)}{1\ \text{W}\cdot\text{m}^{-1}\cdot\text{K}^{-1}} = F(T)\,(0.09022 + 0.01182T_\text{r}) \times\left(1 - \text{e}^{-\left(\left(T_\text{r}^2+36.44T_\text{r}\right)/119.5\right)} - \sum_{i=1}^{3} C_i\,\text{e}^{-((D_\text{i}-\ln(T_\text{r}))/E_\text{i})^2}\right) \tag{13}$$

Here T_r is the reduced temperature ($T_\text{r} = T/T_\text{crit}$) where T_crit is 32.938 K corresponding to para-hydrogen [45]. Table 9 gives the coefficients for Eq. 13. Roder's correction factor was modified to the following form to account for the high-temperature trend in our data:

$$F(T) = 0.935 + 0.02 \times (T_\text{r} + 3.04)^{0.5} \tag{14}$$

Again, using Hanley's table of theoretical data, the para-enhancement was correlated as a function of temperature as

$$\frac{\Delta\lambda_{\text{p–n}}(T)}{1\ \text{W}\cdot\text{m}^{-1}\cdot\text{K}^{-1}} = 0.02711\text{e}^{-((1.621-\ln(T_\text{r}+0.149))/0.5133)^2} \tag{15}$$

Roder's excess thermal-conductivity term re-expressed using the reduced density $\rho_r = \rho/\rho_\text{crit}$ where ρ_crit is 31.323 $\text{kg}\cdot\text{m}^{-3}$ (i.e., critical density of parahydrogen [45]) and gives

$$\frac{\Delta\lambda_{\text{excess}}(T,\rho)}{1\ \text{W}\cdot\text{m}^{-1}\cdot\text{K}^{-1}} = 0.02465\rho_\text{r} + \delta\left(\text{e}^{5.64\rho_\text{r}^{0.36}} - 1\right) \tag{16}$$

To better account for the trend in our data, the temperature dependence of the excess thermal conductivity was modified to

$$\delta = 4.0\times10^{-5} + 6.5\times10^{-5}\text{e}^{-\left(0.008\times(T_\text{r}-19)^2\right)} \tag{17}$$

Roder's critical enhancement term using non-dimensionalized density and temperature can be expressed as

$$\begin{aligned}\frac{\Delta\lambda_{\text{crit}}(T,\rho)}{1\ \text{W}\cdot\text{m}^{-1}\cdot\text{K}^{-1}} &= (0.006354 - 0.00193T_\text{r})\,\text{e}^{-\left(2.147\left(\rho_\text{r}+0.1(T_\text{r}-1)^{1.5}-1\right)\right)^2} \\ &= 0\,(T_\text{r} > 0.006354/0.00193)\end{aligned} \tag{18}$$

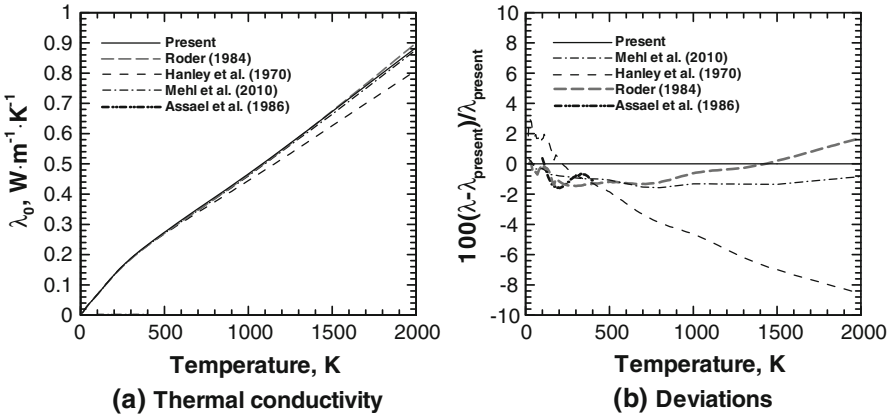

Fig. 13 Dilute-gas thermal conductivity for normal hydrogen

Besides replacing the tabulated data of Hanley et al. [44] with Eqs. 13 and 15, the main difference between the present correlation and that of Roder [11] is the changed functional forms for Eqs. 14 and 17.

Before discussing the present data, it is worthwhile to compare Eq. 13 with Roder's dilute gas correlation and theoretical data including the latest calculations for dilute hydrogen gas by Mehl et al. [10]. This comparison is shown in Fig. 13. Generally, the present correlation is about 1 % higher than the data of Mehl et al. [10] and also initially about 1.5 % higher than Roder's empirical correction [11] to Hanley's table [44]. The correlation of Assael et al. [7] is also about 1 % lower than the present correlation in the range of its applicability.

Figure 14 gives a comparison of the present correlation with the present measurements and also with a few selected isotherms from the literature. In order to evaluate the density required in Eqs. 16 and 18 from the temperature and pressure, the equation of state by Leachman et al. [45] was used. Apart from the data corresponding to pressures less than 1 MPa at temperatures higher than 150 °C, the dependence of the thermal conductivity on pressure is well captured by the present correlation. Good agreement can also be observed for the isotherms by Roder [11], Mustafa et al. [14], and Clifford and Gray [16]. The coaxial cylinder data by Hamrin and Thodos [17] show an obvious deviation from the tendencies of the present dataset and the datasets by other authors.

Figure 15 shows the deviations of the present data from the present correlation. It is clear that the majority of the present measurements fall within ±2 % of the correlation. The main exception is the high-temperature data at pressures less than 1 MPa which fall about 4 % lower than the present correlation. The reason for this sudden systematic deviation of the low-density data is unclear. The data of Roder [11,12] are also plotted in Fig. 15 along with data by a number of other authors [13–19]. With the exception of the data by Hamrin and Thodos [17], the very high-temperature data by Saxena and Saxena [19] and the 1970 parallel-plate data by Roder and Diller [13], the majority of the data falls within ±3 % of the present correlation. The large deviation of the liquid-hydrogen data by Roder and Diller [13] show clearly that the present

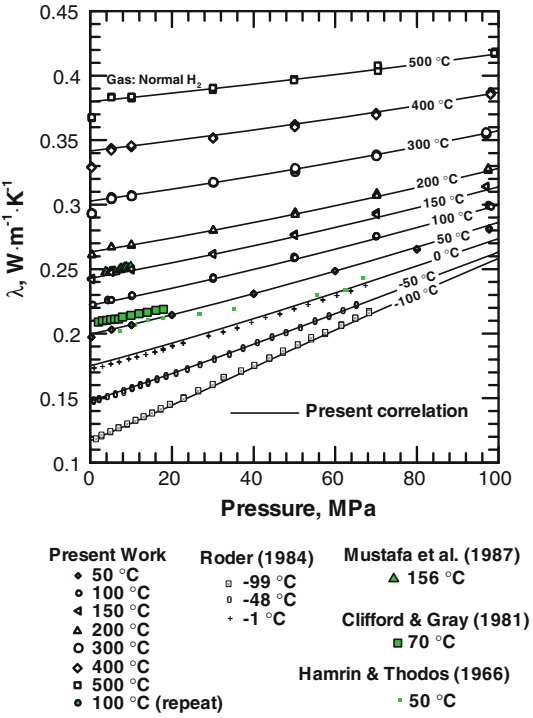

Fig. 14 Isotherms of normal hydrogen thermal conductivity [11,14,16,17] (*solid lines* show present correlation)

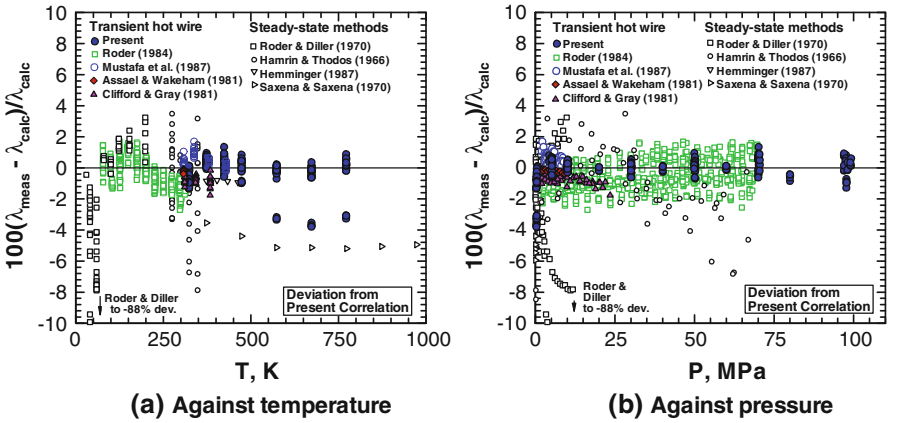

Fig. 15 Deviations of normal hydrogen thermal conductivity [11–19] from the present correlation

correlation is not suitable for the region for $T < 78$ K. Thus, we can conclude that the present correlation is applicable in the range of temperature, 78 K $< T <$ 773 K and pressure, $0 \ll 100$ MPa with an uncertainty of ± 2 % for $T > 323$ K corresponding to the range of data for the present measurements and an uncertainty of ± 3 % for $T < 323$K.

11 Conclusions

Measurements of hydrogen and helium thermal conductivity in the region from 50 °C to 500 °C at pressures from 0.3 MPa to 99 MPa were successfully taken with a transient short hot-wire instrument. The measurements of the thermal conductivity of helium were in agreement with the correlation by Hands and Arp [32] within a deviation of ±3 % for the entire range of temperature and pressure considered. This is an indication of the reliability of the thermal-conductivity measurements for high-pressure high-temperature gases. The hydrogen thermal-conductivity measurements showed a deviation of ±4 % from an extrapolation of Roder's correlation [11] to the high temperature region. A new correlation was developed based on Roder's correlation which is in agreement with the present data within ±2 % except for an anomalous behavior of the low-pressure measurements (<1 MPa) at temperatures above 150 °C.

Acknowledgment This research has been conducted as a part of the "Fundamental Research Project on Advanced Hydrogen Science" funded by the New Energy and Industrial Technology Development Organization (NEDO).

References

1. J.C. Maxwell, in *The Scientific Papers of James Clerk Maxwell*, vol. 2 (Dover, New York, 1965), pp. 26–78
2. D. Zhou, G.G. Ihas, N.S. Sullivan, J. Low Temp. Phys. **134**, 401 (2004)
3. T.W. Bradshaw, J.O.W. Norris, Rev. Sci. Instrum. **58**, 83 (1987)
4. O.F. Degtyareva, L.T. Bondareva, J. Anal. Chem. **59**, 442 (2004)
5. F.N. Edmonds, Astrophys. J. **125**, 535 (1957)
6. J.W. Leachman, R.T. Jacobsen, S.G. Penoncello, M.L. Huber, Int. J. Thermophys. **28**, 773 (2007)
7. M.J. Assael, S. Mixafendi, W.A. Wakeham, J. Phys. Chem. Ref. Data **15**, 1315 (1986)
8. R.D. McCarty, J. Hord, H.M. Roder. *Selected Properties of Hydrogen (Engineering Design Data)*. National Bureau of Standards Monograph 168 (U.S. Government Printing Office, Washington, DC, 1981)
9. R.D. McCarty. *Hydrogen Technological Survey—Thermophysical Properties*. National Aeronautics and Space Administration (NASA) Monograph SP-3089 (NASA, Washington, DC, 1975)
10. J.B. Mehl, M.L. Huber, A.H. Harvey, Int. J. Thermophys. **31**, 740 (2010)
11. H.M. Roder, Int. J. Thermophys. **5**, 323 (1984)
12. H.M. Roder, *Experimental Thermal Conductivity Values for Hydrogen, Methane and Ethane*, National Bureau of Standards Interagency Report NBSIR 84-3006 (National Bureau of Standards, Boulder, CO, 1984)
13. H.M. Roder, D.E. Diller, J. Chem. Phys. **52**, 5928 (1970)
14. M. Mustafa, M. Ross, R.D. Trengove, W.A. Wakeham, M. Zalaf, Physica **141**, 233 (1987)
15. M.J. Assael, W.A. Wakeham, J. Chem. Soc., Faraday Trans. 1 **77**, 697 (1981)
16. A.A. Clifford, P. Gray, J. Chem. Soc., Faraday Trans. 1 **77**, 2679 (1981)
17. C.E. Hamrin, G. Thodos, Physica **32**, 918 (1966)
18. W. Hemminger, Int. J. Thermophys. **8**, 317 (1987)
19. S.C. Saxena, V.K. Saxena, J. Phys. A: Gen. Phys. **3**, 309 (1970)
20. D.L. Timrot, A.S. Umanskii, High Temp. **4**, 285 (1966)
21. M. Fujii, X. Zhang, N. Imaishi, S. Fujiwara, T. Sakamoto, Int. J. Thermophys. **18**, 327 (1997)
22. X. Zhang, W. Hendro, M. Fujii, T. Tomimura, N. Imaishi, Int. J. Thermophys. **23**, 1077 (2002)
23. P.L. Woodfield, J. Fukai, M. Fujii, Y. Takata, K. Shinzato, Int. J. Thermophys. **29**, 1299 (2008)
24. P.L. Woodfield, J. Fukai, M. Fujii, Y. Takata, Int. J. Thermophys. **30**, 796 (2009)
25. P.L. Woodfield, S. Moroe, J. Fukai, M. Fujii, K. Shinzato, M. Kohno, Y. Takata, Int. J. Thermophys. **30**, 1748 (2009)

26. M.J. Assael, C.A. Nieto de Castro, H.M. Roder, W.A. Wakeham, in *Experimental Thermodynamics, Measurement of the Transport Properties of Fluids*, vol. III, ed. by W. Wakeham, A. Nagashima, J.V. Sengers (Blackwell Scientific, Oxford, 1991)
27. S. Moroe, P.L. Woodfield, J. Fukai, K. Shinzato, M. Kohno, M. Fujii, Y. Takata, Exp. Heat Transfer **24**, 168 (2011)
28. X. Zhang, S. Fujiwara, Z. Qi, M. Fujii, J. Jpn. Soc. Microgravity Appl. **16**, 129 (1999)
29. M.L.V. Ramires, C.A. Nieto de Castro, R.A. Perkins, Y. Nagasaka, A. Nagashima, M. Assael, W.A. Wakeham, J. Phys. Chem. Ref. Data **29**, 133 (2000)
30. E.F. May, R.F. Berg, M.R. Moldover, Int. J. Thermophys. **28**, 1085 (2007)
31. J.J. Hurly, M.R. Moldover, J. Res. Natl. Inst. Stand. Technol. **105**, 667 (2000)
32. B.A. Hands, V.D. Arp, Cryogenics **22**, 697 (1981)
33. NIST Standard Reference Database 69: NIST Chemistry WebBook (National Institute of Standards and Technology, Gaithersburg, MD, 2008), http://webbook.nist.gov/chemistry/
34. E. Bich, J. Millat, E. Vogel, J. Phys. Chem. Ref. Data **19**, 1289 (1990)
35. J. Kestin, K. Knierim, E.A. Mason, B. Najafi, S.T. Ro, M. Waldman, J. Phys. Chem. Ref. Data **13**, 229 (1984)
36. M.J. Assael, M. Dix, A. Lucas, W.A. Wakeham, J. Chem. Soc., Faraday Trans. 1 **77**, 439 (1981)
37. J. Kestin, R. Paul, A.A Clifford, W.A. Wakeham, Physica **100**, 349 (1980)
38. R.D. McCarty, V.D. Arp, Adv. Cryog. Eng. **35**, 1465 (1990)
39. V.D. Arp, R.D. McCarty, *NIST Technical Note 1334* (U.S. Government Printing Office, Washington, DC, 1989)
40. M. Jaeschke, P. Schley, Int. J. Thermophys. **16**, 1381 (1995)
41. H.M. Roder, C.A. Nieto de Castro, Cryogenics **27**, 312 (1987)
42. ISO/IEC Guide 98-3:2008, *Uncertainty of Measurement—Part 3: Guide to the Expression of Uncertainty in Measurement (GUM: 1995)* (ISO, Geneva, Switzerland, 2008), http://www.iso.org/sites/JCGM/GUM-JCGM100.htm
43. L. Sun, J.E.S. Venart, R.C. Prasad, Int. J. Thermophys. **23**, 357 (2002)
44. H.J.M. Hanley, R.D. McCarty, H. Intemann, J. Res. Natl. Bur. Stand. **74**, 331 (1970)
45. J.W. Leachman, R.T. Jacobsen, S.G. Penoncello, E.W. Lemmon, J. Phys. Chem. Ref. Data **38**, 721 (2009)